UNIVERSITY OF LEEDS

This is a repository copy of *Probabilistic analysis and comparison of stress-dependent rock physics models*.

White Rose Research Online URL for this paper:
http://eprints.whiterose.ac.uk/115104/

Version: Accepted Version

Article:
Price, DC, Angus, DA, Garcia, A et al. (1 more author) (2017) Probabilistic analysis and comparison of stress-dependent rock physics models. Geophysical Journal International, 210 (1). pp. 196-209. ISSN 0956-540X

https://doi.org/10.1093/gji/ggx151

© The Authors 2017. Published by Oxford University Press on behalf of The Royal Astronomical Society. This is a pre-copyedited, author-produced PDF of an article accepted for publication in Geophysical Journal International following peer review. The version of record, 'Price, DC, Angus, DA, Garcia, A and Fisher, QJ (2017) Probabilistic analysis and comparison of stress-dependent rock physics models. Geophysical Journal International, 210 (1). pp. 196-209,' is available online at:
https://doi.org/10.1093/gji/ggx151

Reuse
Unless indicated otherwise, fulltext items are protected by copyright with all rights reserved. The copyright exception in section 29 of the Copyright, Designs and Patents Act 1988 allows the making of a single copy solely for the purpose of non-commercial research or private study within the limits of fair dealing. The publisher or other rights-holder may allow further reproduction and re-use of this version - refer to the White Rose Research Online record for this item. Where records identify the publisher as the copyright holder, users can verify any specific terms of use on the publisher's website.

Takedown
If you consider content in White Rose Research Online to be in breach of UK law, please notify us by emailing eprints@whiterose.ac.uk including the URL of the record and the reason for the withdrawal request.

White Rose university consortium
Universities of Leeds, Sheffield & York

eprints@whiterose.ac.uk
https://eprints.whiterose.ac.uk/

submitted to *Geophys. J. Int.*

Probabilistic analysis and comparison of stress-dependent rock physics models

D.C. Price[1], D.A. Angus[1,2], A. Garcia[3] & Q.J. Fisher[1]

[1] *School of Earth & Environment, University of Leeds, Leeds, UK*

[2] *Now at: ESG Solutions, Kingston, Canada*

[3] *Total E&P UK Limited, Geoscience Research Centre, Aberdeen, UK.*

SUMMARY

A rock physics model attempts to account for the nonlinear stress-dependence of seismic velocity by relating changes in stress and strain to changes in seismic velocity and anisotropy. Understanding and being able to model this relationship is crucial for any time-lapse geophysical or geo-hazard modelling scenario. In this study, we take a number of commonly used rock physics models and assess their behaviour and stability when applied to stress versus velocity measurements of a large (dry) core dataset of different lithologys. We invert and calibrate each model and present a database of models for over 400 core samples. The results of which provide a useful tool for setting a priori parameter constraints for future model inversions. We observe that some models assume an increase in V_P/V_S ratio (hence Poisson's ratio) with stress. A trait not seen for every sample in our dataset. We demonstrate that most model parameters are well constrained. However, third order elasticity models become ill-posed when their equations are simplified for an isotropic rock. We also find that third order elasticity models are limited by their approximation of an exponential relationship via functions that lack an exponential term. We also argue that all models are difficult to parameterise without the availability of core data. Therefore, we derive simple relationships between model parameters, core porosity

and clay content. We observe that these relationship are suitable for estimating seismic velocities of rock but poor when comes to predicting changes related to effective stress. The findings of this study emphasise the need for improvement to models if quantitatively accurate predictions of time-lapse velocity and anisotropy are to be made. Certain models appear to better fit velocity depth log data than velocity-stress core data. Thus, there is evidence to suggest a limitation in core data as a representation of the stress dependence of the subsurface. The differences in the stress-dependence of the subsurface compared to that measured under laboratory conditions could potentially be significant. Although potentially difficult to investigate, its importance is of great significance if we wish to accurately interpret the stress dependence of subsurface seismic velocities.

Key words: Non-linear rock physics models, Parameter Inversion, Probability

1 INTRODUCTION

The presence of cracks (e.g., faults, fractures, joints and micro-cracks) in brittle rock results in a non-linear relationship between effective stress and rock elasticity (e.g., Walsh, 1965a ; Walsh, 1965b). The presence of cracks and pore pressure play a significant role in the geomechanical response of the subsurface (e.g., Zoback, 2010 ; Cornet, 2015) because the effective stress field is heavily influenced by pore pressure (Terzaghi, 1943). At relatively low stresses (i.e. shallow crustal depths), this non-linear relationship is governed by the displacement discontinuity introduced by cracks; and the stress-dependence of crack stiffness, related to the complex heterogeneous geometry of the crack surface. This relationship between effective stress and geomechanical behaviour leads to a nonlinear stress-dependence of seismic velocity (e.g., Nur and Simmons, 1969) and seismic anisotropy (e.g., Crampin, 2005 ; Baird et al., 2013a). This has important implications for geophysical (e.g. hydrocarbon reservoirs and CO_2 storage) and geo-hazard (e.g., volcanology and earthquake) monitoring scenarios.

Stress-dependent rock physics models aim to account for this nonlinearity by relating changes in stress and strain to seismic velocity and anisotropy. Effectively, these models are based on the recognition that an increase in effective stress will result in a non-linear increase in seismic velocity due to closure of cracks, grain boundaries and discontinuities. The non-linear (i.e. exponential) behaviour is a consequence of a greater number of more compliant cracks at lower effective stresses. Many models have been derived to account for this non-linearity, such as empirically determined relation-

ships (e.g., Zimmerman et al., 1986), third order elasticity theory (e.g., Prioul et al., 2004 ; Korneev & Glubokovskikh, 2013), Hertz-Mindlin contact forces (e.g., Makse et al., 1999), micro-structural models (e.g., Sayers, 2002 ; Tod, 2002 ; Hall et al., 2008 ; Sarout & Guéguen, 2008 ; Ougier-Simonin et al., 2009 ; Guéguen & Sarout, 2011) and relationships derived from first principles that are consistent with empirically derived equations (e.g., Shapiro, 2003 ; Shapiro, 2005).

Rock physics models have recently become increasingly important in the hydrocarbon industry as a method of modelling the influence of production related stress changes on seismic velocities (e.g., Guilbot and Smith, 2002 ; Herwanger and Koutsabeloulis, 2011 ; Angus et al., 2015). Angus et al., 2009 and Angus et al., 2012 used a large dataset (> 200) of ultrasonic velocity versus stress measurements of sedimentary core samples to constrain the micro-structural rock physics models of Sayers, 2002 and Tod, 2002. From these studies, plausible values of model parameters were established for various rock lithology. Each model gave a relatively good fit to the observed data and were subsequently used in hydrocarbon time-lapse prediction (e.g., Angus et al., 2015).

Although such studies are useful for establishing different model formulations, little research has been conducted on model stability and robustness. In this study we take a number of commonly used rock physics models and vigorously assess their behaviour and stability when applied to stress versus velocity measurements of a large (dry) core dataset of different lithologies. Specifically, using a collection of ultrasonic velocity versus stress measurements we invert for various model parameters. We then critically analyse the fit of each model to the observed data and compare their time-lapse velocity predictions when subject to a typical hydrocarbon scenario. The inversion constraint is also simultaneously assessed using Bayesian style statistics. Finally, we use the inversion results to derive parameter-porosity-clay relationships to assess the potential calibration of models when laboratory measurements are unavailable (i.e. calibrate models using rock properties measurable from wellbore data).

2 ROCK PHYSICS MODELS

There are many different rock physics models available, each aiming to relate changes in stress and strain to seismic velocity. However, since there are many different mathematical formulations, it is not feasible to collate and analyse each published relationship. Instead, we focus our attention to the most common theorems and formulae used for hydrocarbon monitoring scenarios. A total of 5 different models are analysed: an empirical (EMP) model (e.g., Zimmerman et al., 1986), a first principle (FPR) model (e.g., Shapiro, 2003), a micro-structural (MST) model (e.g., Schoenberg and Sayers, 1995) and two third-order elasticity (TOE) models (e.g., Prioul et al., 2004 ; Korneev & Glubokovskikh, 2013).

It should be noted that the development of new cracks or the permanent deformation of pre-existing cracks and pores are not considered in certain models (i.e. no hysteretic behaviour). Although the influence of plastic deformation could be modelled using porosity-velocity relationships (e.g., Avseth et al., 2010), these transforms may neglect important geomechanical effects such as shear-banding. As well, we assume that the ultrasonic velocity relationships are a good representation of velocity-stress relationships at seismic frequencies. It is recognised that there is indeed a frequency dependence but that is beyond the scope of this paper.

2.1 Empiricle (EMP) Model

Zimmerman et al., 1986 propose that for an isotropic rock under an isotropic load the seismic velocity V_ν (where ν refers to either the P- or S-wave) can be related to the effective stress σ via

$$V_\nu(\sigma) = A_\nu + K_\nu\sigma - B_\nu \exp(-\sigma D_\nu), \tag{1}$$

where A_ν, K_ν, B_ν and D_ν are material dependent coefficients (or fitting parameters) which can differ for P- and S-waves. If the effective stress is on the order of MPa (which is often the case for geophysical and geo-hazard scenarios), the second term in equation 1 becomes orders of magnitude less than the other two terms and thus can be neglected (e.g., Zimmerman et al., 1986 ; Eberhart-Phillips et al., 1989 ; Khaksar et al., 1999 ; Kirstetter & MacBeth, 2001),

$$V_\nu(\sigma) = A_\nu - B_\nu \exp(-\sigma D_\nu). \tag{2}$$

Equation 2 generally provides a good approximation for both dry and saturated rocks (e.g., Jones, 1995). This is due to the fact that the model fits an exponential curve to data that typically displays an exponential trend. However, this model is limited in that its material dependent coefficients lack any physical meaning and are often empirically determined (e.g., Eberhart-Phillips et al., 1989).

2.2 First Principle (FPR) Model

Shapiro, 2003 expands on the formulation of Zimmerman et al., 1986 by deriving physical meanings for the model coefficients A_ν, K_ν, B_ν and D_ν. Shapiro, 2003 assumes that the stress dependence of porosity controls the change in elastic moduli and that the total porosity ϕ is a function of both compliant ϕ_c and stiff ϕ_s porosity terms,

$$\phi = \phi_c + \phi_s. \tag{3}$$

The compliant porosity consists of thin cracks and open spaces within grain contact boundaries, whereas the stiff porosity consists of the approximately spherical pores. Although compliant porosity

makes up only a small percentage of the overall pore space, its relative change with stress is far greater than the relative change in stiff porosity.

Shapiro, 2003 uses the theory of poro-elasticity to derive an exponential relationship between compliant porosity and applied effective stress,

$$\phi_c = \phi_c^0 \exp(-\theta_c \sigma / K^*), \tag{4}$$

where ϕ_c^0 is the compliant porosity at zero effective stress and K^* the bulk modulus of a rock assuming zero compliant porosity (i.e. a perfectly linear elastic rock with no cracks). The term θ_c represents a so-called elastic piezo-sensitivity coefficient

$$\theta_c = \frac{K_g(3K_g + 4\mu_g)}{\pi a \mu_g (3K_g + \mu_g)}, \tag{5}$$

where K_g and μ_g are the bulk and shear moduli of the grain material respectively, and a the effective aspect ratio of the compliant pore space. Based on these equations Shapiro, 2003 expresses the velocity as a function of compliant porosity,

$$V_P(\sigma) \approx V_P^* - \frac{1}{2} V_P^* H_c \theta_{c\mu} \phi_c \tag{6}$$

and

$$V_S(\sigma) \approx V_S^* - \frac{1}{2} V_S^* \theta_{c\mu} \phi_c, \tag{7}$$

where V_P^* and V_S^* are the P- and S-wave velocity of the zero compliant porosity rock. The parameters $\theta_{c\mu}$ and H_c are defined as

$$\theta_{c\mu} \approx \frac{1}{5}\left[1 + \frac{4(3K_g + 4\mu_g)(9K_g + 4\mu_g)}{3\pi a (3K_g + \mu_g)(3K_g + 2\mu_g)}\right] \tag{8}$$

and

$$H_c = \frac{K^* \theta_c / \theta_{c\mu} + 4\mu^*/3}{K^* + 4\mu^*/3}, \tag{9}$$

where μ^* is the shear modulus of the zero compliant porosity rock. Note that again the linear K_ν term is left out of equations 6 and 7. Shapiro, 2003 expresses this term as a function of the stiff porosity ϕ_s and makes the same observation as Zimmerman et al., 1986 in that it can be neglected in comparison to the two other, much larger terms. Shapiro, 2003 also states that the exponential term in equation 4 is constant for both the P- and S-wave velocities and that equations 6 and 7 are valid for both dry and saturated rocks.

2.3 Microstructural (MST) Model

Schoenberg and Sayers, 1995 introduced an excess compliance approach to model the influence of cracks. The elastic compliance of a rock S_{ijkl} (the inverse of elasticity C_{ijkl}) can be thought of as

being the sum of the intrinsic compliance of the rock matrix (in the absence of discontinuities) S^0_{ijkl}, plus the additional extrinsic compliance ΔS_{ijkl} due to the presence of cracks and grain contacts

$$S_{ijkl} = S^0_{ijkl} + \Delta S_{ijkl}. \tag{10}$$

The excess compliance due to cracks ΔS_{ijkl} can be expressed in terms of a second- and a fourth-rank crack density tensor α_{ij} and β_{ijkl}

$$\Delta S_{ijkl} = \frac{1}{4}(\delta_{ik}\alpha_{jl} + \delta_{il}\alpha_{jk} + \delta_{jk}\alpha_{il} + \delta_{il}\alpha_{ik}) + \beta_{ijkl}, \tag{11}$$

where δ_{ij} is the Kronecker delta. The second- and fourth-rank crack density tensors are defined

$$\alpha_{ij} = \frac{1}{V}\sum_m B^m_T n^m_i n^m_j S^m \tag{12}$$

and

$$\beta_{ijkl} = \frac{1}{V}\sum_m (B^m_N - B^m_T) n^m_i n^m_j n^m_k n^m_l S^m, \tag{13}$$

where V is volume and B^m_N and B^m_T the normal and tangential crack compliance across the m–th displacement discontinuity having unit normal n_i and surface area S^m. Note that summation convention is used for equations 10-13.

Sayers and Kachanov, 1995 state that as the ratio of normal to tangential crack compliance $B_N/B_T \rightarrow 1$ (i.e. as $B_N \rightarrow B_T$), the fourth-rank crack density tensor β_{ijkl} becomes at least an order of magnitude smaller than the second-rank crack density tensor α_{ij}. When $B_N/B_T = 1$, the so-called scalar crack assumption, $\beta_{ijkl} = 0$ and any crack set can be described by the three orthogonal components of the second-rank crack tensor α_{ij}. It has been shown that the scalar crack assumption is not universally valid for most real rocks (e.g., Angus et al., 2009 ; Angus et al., 2012 ; Choi et al., 2014). However, Hall et al., 2008 and Verdon et al., 2008 observe that the scalar crack assumption is still a valid approximation to predict the general characteristics of stress dependent velocity and anisotropy. They provide a set of equations that express the nine independent elastic constants of the orthorhombic stiffness tensor C_{ij} in terms of the second-rank crack tensor α_{ij} and the compliance tensor of the

background medium S^0_{ij} (i.e. rock mineral components),

$$\begin{aligned}
C_{11} &= [(S^0_{23})^2 - (S^0_{22}+\alpha_{22})(S^0_{33}+\alpha_{33})]/D \\
C_{22} &= [(S^0_{13})^2 - (S^0_{11}+\alpha_{11})(S^0_{33}+\alpha_{33})]/D \\
C_{33} &= [(S^0_{12})^2 - (S^0_{11}+\alpha_{11})(S^0_{22}+\alpha_{22})]/D \\
C_{12} &= [S^0_{12}(S^0_{33}+\alpha_{33}) - S^0_{13}S^0_{23}]/D \\
C_{13} &= [S^0_{13}(S^0_{22}+\alpha_{22}) - S^0_{12}S^0_{23}]/D \\
C_{23} &= [S^0_{23}(S^0_{11}+\alpha_{11}) - S^0_{12}S^0_{13}]/D \\
C_{44} &= [S^0_{44}+\alpha_{22}+\alpha_{33}]^{-1} \\
C_{55} &= [S^0_{55}+\alpha_{11}+\alpha_{33}]^{-1} \\
C_{66} &= [S^0_{66}+\alpha_{11}+\alpha_{22}]^{-1},
\end{aligned} \tag{14}$$

where

$$\begin{aligned}
D =&(S^0_{11}+\alpha_{11})(S^0_{23})^2 + (S^0_{22}+\alpha_{22})(S^0_{13})^2 + \\
&(S^0_{33}+\alpha_{33})(S^0_{12})^2 - 2S^0_{12}S^0_{13}S^0_{23} - \\
&(S^0_{11}+\alpha_{11})(S^0_{22}+\alpha_{22})(S^0_{33}+\alpha_{33}).
\end{aligned} \tag{15}$$

The P-wave speeds along the principle axes can be related to the diagonal elements of C_{ij} via

$$V_{11} = \sqrt{\frac{C_{11}}{\rho}}, \quad V_{22} = \sqrt{\frac{C_{22}}{\rho}}, \quad V_{33} = \sqrt{\frac{C_{33}}{\rho}}, \tag{16}$$

and S-waves propagating in the ith direction polarized in the jth by

$$V_{32} = V_{23} = \sqrt{\frac{C_{44}}{\rho}}, \quad V_{31} = V_{13} = \sqrt{\frac{C_{55}}{\rho}}, \quad V_{12} = V_{21} = \sqrt{\frac{C_{66}}{\rho}}. \tag{17}$$

The micro-structural formulation of Sayers, 2002 and Hall et al., 2008 provides only a single second- and fourth-rank crack density value per stress measurement (i.e. no velocity-stress dependence). However, invoking the scalar crack assumption, Tod, 2002 derives an analytical expression for the second-rank crack density, α_{ij} as a function of effective crack normal stress

$$\alpha_{ij} = \begin{cases} \frac{\epsilon_i(\sigma(n_i))}{h_i}, & \text{if } i = j \\ 0, & \text{if} i \neq j \end{cases} \tag{18}$$

where

$$\epsilon_i\left(\sigma(n_i)\right) = \epsilon^0 \exp\left[-\frac{2(1-\nu_b)}{\pi\mu_b a^0}\sigma(n_i)\right]. \tag{19}$$

The terms a^0 and ϵ^0 are the initial aspect ratio and initial crack density at zero applied stress. The parameters ν_b and μ_b are the Poisson's ratio and shear modulus of the matrix assuming a zero compliant

porosity rock. The normalisation term (Schubnel and Gueguen, 2003) h_i is given by

$$h_i = \frac{3E_i(2-\nu_i)}{32(1-\nu_i^2)}. \tag{20}$$

If we assume the rock is isotropic, the second-rank crack density tensor α_{ij} (equation 18) and the normalisation constant h_i (equation 20) can be simplified

$$\alpha_{11} = \alpha_{22} = \alpha_{33} \tag{21}$$

and

$$h_1 = h_2 = h_3. \tag{22}$$

It should be noted that there is often criticism of rock physics models such as the FPR and MST models based on their model idealisations of the rock architecture. It is important to stress that ultrasonic seismic signals are band-limited (i.e. finite frequency bandwidth) and so carry limited information such as travel-time, amplitude and phase. For wave propagation scenarios, such as ultrasonic measurements, the seismic wavefield experiences the averaging effects of sub-wavelength scale features in the rock. Thus, the information that the seismic wavefield provides is not at all comparable to actual rock architecture. However, rock physics models such as the FPR and MST models allow us to construct intuitive model idealisations that have some correlation to measurable parameters.

2.4 Third-Order Elasticity (TOE) Models

Third order elasticity rock physics models present a non-linear elastic stiffness tensor as a function of stress and strain by invoking elasticity theory (e.g., Thurston and Brugger, 1964). They include cubic (or third-rank) terms that account for a non-linear change in stiffness with stress. Third order elastic constants can have different relationships with rock parameters (e.g., Sinha & Plona, 2001 ; Shapiro, 2005 ; Fuck & Tsvankin., 2009). However, in this study we focus primarily on the commonly used TOE models of Prioul et al., 2004 and Korneev & Glubokovskikh, 2013.

2.4.1 TOE-1 Prioul

Prioul et al., 2004 derived nine independent components of an orthorhombic stiffness tensor C_{ij} as

$$\begin{aligned}
C_{11} &= C_{11}^{\text{ref}} + c_{111}\Delta\varepsilon_{11} + c_{112}(\Delta\varepsilon_{22} + \Delta\varepsilon_{33}) \\
C_{22} &= C_{11}^{\text{ref}} + c_{111}\Delta\varepsilon_{22} + c_{112}(\Delta\varepsilon_{11} + \Delta\varepsilon_{33}) \\
C_{33} &= C_{33}^{\text{ref}} + c_{111}\Delta\varepsilon_{33} + c_{112}(\Delta\varepsilon_{11} + \Delta\varepsilon_{33}) \\
C_{12} &= C_{12}^{\text{ref}} + c_{112}(\Delta\varepsilon_{11} + \Delta\varepsilon_{22}) + C_{123}\Delta\varepsilon_{33} \\
C_{13} &= C_{13}^{\text{ref}} + c_{112}(\Delta\varepsilon_{11} + \Delta\varepsilon_{33}) + C_{123}\Delta\varepsilon_{22} \\
C_{23} &= C_{13}^{\text{ref}} + c_{112}(\Delta\varepsilon_{22} + \Delta\varepsilon_{33}) + C_{123}\Delta\varepsilon_{11} \\
C_{44} &= C_{44}^{\text{ref}} + c_{144}\Delta\varepsilon_{11} + c_{155}(\Delta\varepsilon_{22} + \Delta\varepsilon_{33}) \\
C_{55} &= C_{44}^{\text{ref}} + c_{144}\Delta\varepsilon_{22} + c_{155}(\Delta\varepsilon_{11} + \Delta\varepsilon_{33}) \\
C_{66} &= C_{66}^{\text{ref}} + c_{144}\Delta\varepsilon_{33} + c_{155}(\Delta\varepsilon_{11} + \Delta\varepsilon_{22}),
\end{aligned} \tag{23}$$

where rock stiffness is expressed as a function of the second-rank elastic constants of the rock in a fixed reference state C_{ij}^{ref}. $\Delta\varepsilon_{ij}$ is the change in strain as a result of deviations from the reference state and c_{ijk} are third-rank (non-linear) elastic coefficients that define the linear relationship (or gradient) between stiffness and strain. Assuming the third-rank tensor is isotropic, only three independent non-linear coefficients are needed: c_{111}, c_{112} and c_{123}. The remaining two coefficients are given by

$$c_{144} = \frac{(c_{112} - c_{123})}{2}, \quad \text{and} \quad c_{155} = \frac{(c_{111} - c_{112})}{4}. \tag{24}$$

Equation 23 can be simplified further if we assume hydrostatic strain

$$\Delta\varepsilon_{11} = \Delta\varepsilon_{22} = \Delta\varepsilon_{33}. \tag{25}$$

Application of these equations requires strain data, which is often not measured during ultrasonic velocity-stress experiments (e.g., none of the datasets compiled in Angus et al., 2009 ; Angus et al., 2012 , provide strain data). However, Lei et al., 2012 provided an approximation of strain by assuming a hydrostatic stress state and a linear relationship between incremental changes in stress $\Delta\sigma$ and strain $\Delta\varepsilon$,

$$\Delta\varepsilon = \frac{2C_{44}^{\text{ref}}\Delta\sigma}{2C_{44}^{\text{ref}}(3C_{11}^{ref} - 4C_{44}^{\text{ref}})}. \tag{26}$$

Similar to the micro-structural formulation of Sayers, 2002 and Hall et al., 2008 (equation 14), this third-order elasticity model has limited predictive capabilities. Specifically, this particular model is a local linear approximation of a non-linear relationship. However, Prioul et al., 2004 separated the data into several linear stress regimes to provide an approximate yet predictive algorithm.

2.4.2 TOE-2 Korneev & Glubokovskikh

Korneev & Glubokovskikh, 2013 used nonlinear elasticity theory to derive a set of equations that

describe the P- and S-wave velocities of a transversely isotropic medium,

$$V_{11}^2 = V_{22}^2 = V_{0_{11}}^2 + \frac{2q(B+C)}{\rho}, \tag{27}$$

$$V_{33}^2 = V_{0_{33}}^2 + \frac{2q(A+3B+C)}{\rho}, \tag{28}$$

$$V_{13}^2 = V_{31}^2 = V_{23}^2 = V_{32}^2 = V_{0_{13}}^2 + \frac{q(B+\frac{A}{2})}{\rho}, \tag{29}$$

$$V_{12}^2 = V_{21}^2 = V_{0_{12}}^2 + \frac{qB}{\rho}, \tag{30}$$

where A, B and C are TOE constants, ρ is density and $V_{0_{ij}}$ the seismic velocity of the unstressed rock. The parameter q defines a nonlinear static-strain component

$$q = -\frac{\lambda+2\mu}{4(A+3B+C)}\left[1-\sqrt{1-\frac{8(A+3B+C)\sigma}{(\lambda+2\mu)^2}}\right], \tag{31}$$

where λ and μ are the Lamé parameters of the unstressed rock and σ the effective stress. Korneev & Glubokovskikh, 2013 evaluated their analytical formulae using sonic log data and stacking velocities. The results of which showed relatively good fit to the observed data. However, they did not apply their formulae to laboratory measured ultrasonic velocity versus stress measurements.

3 CORE DATA

The ultrasonic velocity versus stress measurements used in this study were compiled by Angus et al., 2009. However, we augment this dataset to include sandstone core data complimentary from the Wolfson Multiphase Flow Laboratory of the University of Leeds along with other tight sandstone (Al-Harasi et al., 2013) and shale samples (Lorinczi et al., 2014). The complete dataset is summarised in Table 1. As the majority of published datasets only include a single P- and S-wave velocity measurement along a single direction (i.e. vertical axis of the cylindrical core sample), we use only the vertical velocity measurements of the few multi-directional datasets. If multi-directional data are available, anisotropic rock behaviour and hence anisotropic non-linear model parameters could be considered (e.g., Verdon et al., 2008). However, due to a lack of anisotropic data within this particular dataset, we focus on the isotropic scenario.

4 INVERSION METHODOLOGY

Some of the rock physics models defined in the previous section require some form of information regarding the mineral composition of the sample rock (e.g., K_g and μ_g for the FPR model), or so-called zero compliant porosity elasticity (e.g., V^* for the FPR model, and S^0_{ijkl}, ν_b and μ_b for the

MST model). Typically, these are determined using either quantitative X-ray diffraction methods (e.g., Kendall et al., 2007) or estimated from the behaviour of the rock sample at high confining stress (e.g., Sayers, 2002). However, obtaining mineral composition data is not trivial. The utility of using mineral data itself to estimate non-compliant elasticity neglects the importance of cementation and grain packing. This leads to potentially inconsistent or inaccurate velocity estimates. Also, laboratory ultrasonic velocity experiments typically try to minimise plastic deformation and so avoid high effective stresses. This means that the sample likely never reaches the state where all discontinuities are fully closed i.e. zero compliant porosity. As such, in this study we express each of these parameters in terms of the P- and S-wave velocity of a hypothetical rock with zero compliant porosity. We also assume that the velocity of a rock with zero compliant porosity is equal to that of the grain material V_P^{gr}, V_S^{gr}. A valid simplification, supported by equation 9 of Shapiro, 2003, which is based on the observation that for very high stresses the stiff porosity will obey an exponentially decreasing behaviour. However, to constrain the inversion, we assume that these grain velocities (i.e. where $\partial V/\partial\sigma = 0$) are within ± 300 ms^{-1} of the highest recorded stress velocity.

For the TOE-1 model, we follow the approach of Prioul et al., 2004 and separate the data into low ($\sigma \leq 20$ MPa), middle ($20 > \sigma \leq 60$ MPa) and high ($\sigma > 60$ Mpa) stress regimes and invert for the third-rank coefficients of each regime separately. Since a reference rock state is needed (C_{ij}^{ref} in equation 23), a priori knowledge of the second-rank elastic constants of the rock at each stress interval is required. For our case, we assume this to be the data point whose stress value is closest to the lower bound of each interval (i.e. 0 MPa, 20 MPa and 60 MPa). As no strain data is available, we apply the approximation of Lei et al., 2012 (equation 26). Furthermore, as we are considering only vertically propagating P- and S-waves, we consider only equations 27 and 29 from the TOE-2 model of Korneev & Glubokovskikh, 2013. We also jointly invert for the P- and S-wave velocities at zero confining stress ($V_{0_{33}}$ and $V_{0_{13}}$) due to the lack of zero stress velocity measurements. Table 2 provides an overview of all unknown parameters for each of the five models.

For the inversion scheme, we set relatively large (but theoretically acceptable) parameter ranges for the initial inversion. This is because (1) the literature contains sparse information regarding definitive model parameter ranges and (2) we seek to study model robustness and how well constrained the model inversions are. Since we set some of the parameter ranges to span large orders of magnitude we use the Neighbourhood Algorithm (NA) of Sambridge, 1999a as the inversion procedure. The NA discretises the parameter space using Voronoi cells and iteratively explores the cells (or 'neighbourhoods') that appear the most promising. This results in a model ensemble that has sparse coverage over a broad range of the parameter space, whilst much finer i.e. localized, coverage near minima in the misfit function. This makes it an ideal algorithm to use for potentially very sharp global minima

in a misfit function that may span many orders of magnitude. We define the objective function as the model misfit between either both the P- and S-wave data or separately for each wave. The parameters for the NA global search are kept constant for all samples and models such that the inversion results can be compared directly. For each sample, once an appropriate model solution has been found, the search ensemble is evaluated using the method of Sambridge, 1999b. This algorithm was developed as a compliment to the NA sample and implements a Bayesian integration of the NA ensemble. It calculates 1D and 2D probability density functions (PDFs), to explore the confidence in any given coefficient or trade-off between different parameters.

5 RESULTS

Here we present the inversion results of each rock physics model and analyse their fit to the observed data. We also compare each models time-lapse velocity predictions when subject to a typical hydrocarbon scenario. The constraint of each model inversion is analysed and we present a collection of 1D and 2D PDFs of different model parameters. Finally, we derive simple relationships between model parameters and key rock properties. These results then used to discuss the potential calibration of certain models to predict suitably accurate time-lapse changes in seismic velocity when laboratory measurements are unavailable.

5.1 Initial Inversion Results

Figure 1 shows the inversion results for a single sandstone core sample and is a good representation of the whole dataset. Specifically, the results across each model show successful optimisation and a suitably good fit to the observed data. The inversion results for all samples are shown in the histograms of Figure 2. Care must be taken when interpreting these results as the dataset contains an unequal distribution of core samples of differing rock lithology. Therefore it should primarily be used to assess the range of values found for each parameter across our dataset. It should be noted that due to the limited number of high stress measurements, there are fewer values for the TOE-1 model high stress regime (i.e. mainly the hard rock samples have measurements above 60 MPa).

If we examine each model fit to the observed data in more detail we observe that the TOE-2 model provides a relatively poor fit to observed P-wave velocity data at high effective stresses. Also, we note a slight degradation in most of the MST and FPR S-wave velocity predictions at low effective stress. If we look at the histograms of the EMP model, we see slightly different distributions in parameters A_ν, B_ν and D_ν when used to fit either P- or S-wave data. For the parameter A_ν, a shift in the distribution from P to S is to be expected as the S-wave speed at high stress (i.e. $\sigma \rightarrow \infty$) will be lower

than the corresponding P-wave speed. However, differing distributions of B_ν and D_ν suggests that many samples have a different P- and S-wave velocity stress dependence (i.e. differing curvatures of the velocity-stress relationship). As such, this indicates that the V_P/V_S ratio, and hence Poisson's ratio, is stress dependent. By comparing the V_P/V_S ratio of the data compared to that predicted by the models we see that the FPR, MST and TOE-2 models struggle to fit the observed stress dependent V_P/V_S ratio (e.g., Figure 3). These models appear to be formulated to predict an increase in V_P/V_S ratio with increasing stress (i.e., increase in Poisson's ratio). However, the V_P/V_S ratio of the majority of the samples in our dataset is observed to decrease with increasing stress. By defining model parameters separately for each wave type, the EMP model is more successful in modelling the stress dependent V_P/V_S ratio. If we apply this approach to the FPR, MST and TOE-2 models and invert for model parameters using only a single set of velocity measurements (in this case we choose the P-wave measurements and assume V_S^{gr} is known a priori) we notice a clear improvement in the data fit for a majority of samples (e.g., Figure 4).

Although the results of Figure 4 show that we can improve the fit of the TOE-2 model by using only a single set of velocity measurements, the absolute value of the Root Mean Square Error (RMSE) for the majority of samples is much larger than those seen for other models (see Figure 4). This is due to the fact that the TOE-2 expressions 27 and 29 attempt to model data that display a sharp exponential trend using functions that lack an exponential term. A similar issue is apparent in the TOE-1 model results where the local linear approximation struggles to accurately model the non-linear data. This is especially the case at low effective stresses where the non-linear relationship is at its strongest. Therefore these models yield a relatively poorer fit to the observed data and thus a greater RMSE.

5.2 Model Parameter Constraints

To assess how well constrained each model inversion is, we evaluate the ensemble generated by the NA sampler using the method of Sambridge, 1999b. This approach implements a Bayesian integration of the NA ensemble to produce 1D and 2D Probability Density Functions (PDFs) to explore the confidence in each model parameter. It should be noted that for all models presented in this work we assume no a priori constraint on the unknown parameters and thus assume uniform prior probability density.

Figure 5 show the 1D and 2D PDFs of the P-wave EMP and TOE-1 model of the representative sandstone sample shown in Figure 1. Narrow parameter PDFs for the EMP model highlight a relatively well constrained inversion where only a small subset of the model space can explain the velocity-stress dependence. Whereas, wide TOE-1 parameter PDFs that span the entire model space highlight a relatively poorly constrained inversion. This is a result of an under-determined inverse problem

with no unique solution. A lack of multi-directional velocity data and strain measurements leads to a number of equally well fitted solutions. This is also indicated in the histograms of Figure 2 where the results of the TOE-1 inversion do not display any global trends. Instead they are uniformly spread across the entire model space.

The MST and FPR model show similar results to that of the EMP model, where a well defined global minimum exists in the model space making for a well constrained inversion. Similarly a well constrained inversion is seen for the TOE-2 model if we consider only the P-wave velocity data and the three third order coefficients as a combined unknown function $A + 3B + C$ (Figure 6). However, determining a unique value for each individual third order coefficient i.e. A, B and C, is not possible when considering only a single set of P- and S-wave velocity data. This is shown in the 2D marginals of Figure 6 where a suitably well constrained value of the coefficient A is found but numerous solutions exist for the remaining coefficients B and C which span large orders of magnitude (also seen in the histograms of Figure 2). Therefore, similar to the TOE-1 model, a lack of multi-directional velocity data leads to an under-determined problem with a number of equally well fitted solutions. Although the results presented in Figures 5 and 6 are for a single core sample they are a good representation of the entire dataset. In general we see relatively well constrained EMP, FPR and MST model inversions whilst poorly constrained TOE-1 and TOE-2 inversions.

5.3 Comparison of 4D Predictive Capabilities

Consider a typical hydrocarbon monitoring scenario for a reservoir at a depth of between 2 and 4km. Production related changes in reservoir pore pressure can lead to significant reservoir compaction. This leads to the stretching (i.e. straining) of the overburden and underburden rock mass. Over a production period of 10 to 20 years, reservoir compaction can range from the order of centimetres to meters. This, in turn, can cause a reduction in the effective stress of the surrounding rock mass anywhere from 0.1 to 10MPa (e.g., De Gennaro et al., 2010 ; Herwanger and Koutsabeloulis, 2011). For such a scenario, rock physics models are used as a method of modelling the influence of production related stress change on seismic (i.e. P-wave) velocities (e.g., Hatchell and Bourne, 2005 ; Roste et al., 2006 ; Herwanger and Koutsabeloulis, 2011 ; He et al., 2016). Considering such a scenario, we estimate the percentage change in seismic velocity associated with a 5MPa (i.e. from 35 to 30MPa) reduction in effective stress. We assume that each core sample in our dataset is a potential representation of the velocity-stress dependence and compare the velocity change predicted by each rock physics model. Figure 7 show crossplots of the predicted P-wave velocity results of each model from all samples in our dataset against those predicted by the EMP model. We use the results of the EMP model as a reference here due to it having the lowest RMSE for most core samples. Also it should be noted that

due to degradation in certain model solutions when considering S-wave data (e.g., Figure 4), we take the inversion results for the P-wave only FPR and MST models.

The results show that, in addition to all models having a suitably good fit to the observed data, the FPR, MST and EMP model predict similar changes in seismic velocity with stress. However, it is important to note that slight discrepancies between models do exist. Marked on Figure 7 is a +/- 0.2% region. It is clear that for certain samples these different models do predict up to 0.2% difference in velocity change. As we are dealing with relatively small percentage changes these slight discrepancies between models appear significant. The TOE-1 and TOE-2 models however, appear to overestimate the velocity change for almost all samples. This is due to their poorer fit to the observed data seen across all samples (Figures 1 and 4). Overestimates are caused by these models attempting to fit data that display an exponential trend using functions that lack an exponential term. The poorer fit is emphasised when comparing relatively sensitive measure of velocity change.

5.4 Estimating Model Parameters Using Abundant Rock Properties

Velocity-stress core data is not always readily available. This is often the case for non-reservoir rocks in hydrocarbon scenarios where core samples are not typically taken. Therefore, using core data to invert for a best fitting rock physics model is not always possible. This becomes an issue with models such as the EMP and TOE-1/2 as their coefficients lack physical meaning and thus theoretically cannot be derived without inverting velocity-stress data. On the other hand, the FPR and MST models are parameterised in terms of rock physical properties and thus theoretically can be derived from analysing rock architecture. However, determining properties, such as aspect ratio and crack density, is not trivial and often requires core samples to carry out complex laboratory techniques such as X-ray diffraction.

Eberhart-Phillips et al., 1989 set out to rectify this issue by relating the parameters of the EMP model (equation 1) to more abundant and easily measurable rock properties. Using a dataset of 64 sandstone core samples, Eberhart-Phillips et al., 1989 evaluated the best fitting numerical values for the parameters K, B and D whilst deriving the coefficient A as a function of porosity ϕ and clay content C,

$$V_p = 5.77 - 6.94\phi - 1.73\sqrt{C} + 0.446(\sigma - exp(-16.7\sigma)), \tag{32}$$

and

$$V_s = 3.70 - 4.94\phi - 1.57\sqrt{C} + 0.361(\sigma - exp(-16.7\sigma)). \tag{33}$$

Note that in equations 32 and 33 the P- and S-wave velocities are given in kms^{-1} and the effective stress σ in $kbars$. Eberhart-Phillips et al., 1989 found that these simple approximations give relatively good velocity predictions for their dataset and deduced they may be useful for estimating the veloc-

ity of sandstone rocks for which laboratory measurements are unavailable. However, by replacing the parameters B, D and K with best fitting constants, a constant shape/curvature of the nonlinear relationship must be assumed. Therefore these simple functions may be useful for predicting the absolute magnitude of the rock velocity but may be limited when it comes to describing its nonlinear relationship with stress.

This is demonstrated in Figure 8, where we crossplot, for each sandstone sample in our dataset, the absolute P-wave velocity and it's percentage change associated with a typical hydrocarbon scenario, predicted by equation 32 against those predicted by the original EMP model (equation 2). The hydrocarbon scenario used here is the same as that used for Figure 7. The relatively consistent estimated velocity change across all samples predicted by equation 32 ($\approx 0.5\%$) is an issue for time-lapse seismic monitoring. Estimating accurate time-lapse changes is arguably more important than a good approximation of absolute rock velocity in these scenarios. It should be noted that not all sandstone core samples within our dataset contained information regarding clay content. Therefore this analysis is limited to those sandstone samples in which clay content is available (≈300).

We mimic the procedure taken by Eberhart-Phillips et al., 1989 and aim to relate rock physics model parameters to more abundant rock properties. In this case again porosity and clay content. However, instead of approximating certain parameters with best fitting numerical constants, we aim to relate all unknown parameters to porosity and clay content in an attempt to improve predicted velocity changes. We focus this analysis to purely sandstone samples as they form the majority of the dataset for which clay content and porosity values are available. It is well understood that seismic velocity is a complex function of many rock properties and that it cannot be completely described by porosity and clay content alone (as expressed by Eberhart-Phillips et al., 1989). However, we aim to create simple relationships that could provide useful time-lapse approximations to within a workable accuracy. We calculate linear least squares regression surfaces for each parameter-porosity-clay relationship. The coefficients of each linear model surface, along with its corresponding goodness of fit as an R-squared value, is provided in Table 3. Note that we show the TOE-2 parameters of the P-wave only inversion. This is because it is not possible to define accurate parameter relationships using the results of an unconstrained inversion (e.g., Figure 6). Due to this, the third order coefficients of the TOE-1 model are also excluded (e.g., Figure 5). Figure 9 show crossplots comparing the result of the rock physics model derived from parameter-porosity-clay regression surfaces (predicted) to that derived by the original inversion (base). Presented is the absolute P-wave velocity and its percentage change associated with the same hydrocarbon scenario as that of Figures 7 and 8.

From Table 3 you can see that some parameters show strong parameter-porosity-clay correlations (e.g., V_P^{gr} with R^2 value ≈ 0.8) whilst many show weak or no correlation at all (e.g., ϵ_0 with R^2

value ≈ 0.07). As a result we see in Figure 9 that the models derived from the regression surfaces predict the absolute magnitude of the rock velocity relatively well but are poor when it comes to predicting percentage changes related to stress. Although not shown, little improvement is seen if we fit greater order polynomial surfaces to these poorly correlated parameters. Therefore, it is clear that shape/curvature of the stress-velocity relationship cannot be described by porosity and clay content alone. Little improvement to the predicted velocity change is made by substituting constant terms for porosity-clay relationships.

6 DISCUSSION

A rock physics model is an important component in relating observed time-lapse changes in seismic velocity to changes in stress and strain. It is well known that velocity-stress core data can be used to calibrate models. However, little research has been conducted on their stability and whether they can be calibrated to predict suitable time-lapse changes without the use of laboratory data.

In this study we take some of the most commonly used rock physics models and show that by using velocity-stress core data, each model can be calibrated using similar global search techniques (i.e. the same NA search parameters) to give a relatively good fit to the observed data (e.g., Figure 1). Also, each model appears to predict relatively similar seismic velocity changes when subject to a typical hydrocarbon scenario (e.g., Figure 7). By combining the results of each inversion into the histograms of Figure 2 we present a range of plausible values (across different lithologys) for each model parameter. As literature contains little information regarding definitive parameter ranges, these results may be useful as a prior constraints for future model inversions.

Out of all models studied it appears that the two TOE models possess the least best fit to the overserved data (e.g., Figure 1). As a result, they also appear to consistently overestimate time-lapse velocity changes (e.g., Figure 7). This is due to the TOE-1 model making a linear approximation of a non-linear relationship. Whilst the TOE-2 attempting to model data that typically displays a sharp exponential trend using relationships that lack an exponential term. As the TOE-1 model is a local linear approximation, for practical purposes it requires the velocity-stress relationships to be subdivided into n linear segments. Splitting the data into linear regimes increases model error. This is further compounded since the definitive segment divisions may not be appropriate for all samples given different shape/curvature of the stress-velocity relationship. Furthermore, by subdividing the data into m regimes, the number of model coefficients is increased to $n \times m$. Regardless, the TOE model is still widely used due to its flexibility of allowing general anisotropy (e.g., Herwanger and Koutsabeloulis, 2011) and has been adapted to *in situ* well log measurements (e.g., Donald and Prioul, 2015). The TOE-2 model on the other hand, shows a relatively good fit to velocity depth trends and stacking

velocities (e.g., Korneev & Glubokovskikh, 2013). However, it appears to struggle to fit velocity-stress core data that exhibits a strong exponential trend (e.g., Figure 1). This raises a common question on the validity of stress-velocity core data on its representation of the velocity stress dependence of the subsurface. Is the strong non-linear relationship at low stresses apparent in core data a direct effect of a damaged sample or poor coupling of the transducers to the rock?

We show that the solution to some models (e.g., FPR, MST and TOE-2) is degraded when trying to simultaneously fit both P- and S-wave data (e.g., Figure 4). This is primarily due to these models using the same parameters to model both P- and S-wave behaviour. In doing so, they assume an increase in the V_P/V_S ratio i.e. poisons ratio, with effective stress. However, this is not observed globally across our dataset. Many core samples show an opposing decrease in V_P/V_S ratio with effective stress (e.g., Figure 3). This potentially could be an implication of using an effective medium based approach. However, it is most likely due to the models inability to accurately define the physics on the different interactions that P- and S-waves have with discontinuities. In most monitoring scenarios involving time-lapse seismic data, rock physics models are used predominantly to related changes in stress and strain to seismic i.e. P-wave, velocity. Thus, in these circumstances the use of S-wave data in the inversion process might have a detrimental effect on the model solution (e.g., Figure 4). However, recent application of stress-dependent rock physics models are being used to predict shear-wave anisotropy (e.g., shear-wave splitting) to estimate fracture properties from microseismic data (e.g., Verdon and Wüstefeld, 2013 ; Baird et al., 2013b). Thus, improvements to these models are necessary if quantitatively accurate predictions of S-wave behaviour are needed (e.g. Yousef and Angus, 2016). Furthermore, multi-directional measurements are needed to calibrate the anisotropic model parameters in order to improve predictions of lower-order anisotropic symmetries (e.g., Arts et al., 1992 ; Verdon et al., 2008 ; Nasseri et al., 2013 ; Sarout et al., 2014 ; Sarout et al., 2015).

Many of the models under test in this study appear numerically stable. A relatively well constrained inversion demonstrates that only a small subset of the model space can explain the velocity-stress dependence of each sample (e.g., Figure 5). However, a simplification of the TOE-1 equations (equation 23) for an isotropic rock make the inversion for the three independent third order coefficients, c_{111}, c_{112} and c_{123} ill-posed (e.g., Figure 5). Specifically, the gradient of the linear P-wave velocity-stress relationship is described by the inverse relationship between parameters c_{111} and c_{112}. A similar limitation is seen in the TOE-2 equations where, a lack of multi-directional data, causes an ill-posed inversion for the individual third order coefficients A, B and C (e.g., Figure 6). Therefore it appears for TOE models to be better constrained multi-directional data is required (e.g., Donald and Prioul, 2015).

Finally, we argue in this study that all models under test are difficult to parameterise without the

availability of core data. This becomes an issue for most hydrocarbon scenarios where core samples are not typically taken (especially for non-reservoir rocks). Therefore, deriving a rock physics model in terms of more abundant and easily measurable rock properties is deemed an important research topic. We present the equations of Eberhart-Phillips et al., 1989 (equations 32 and 33) which aim to address this issue by deriving the EMP model in terms of porosity and clay content. However, we show that these relationships are useful for predicting the absolute magnitude of rock velocities but limited in their prediction of time-lapse changes in seismic velocity due to changes in stress (e.g., Figure 7). This is because only certain parameters are related to porosity and clay content whilst others are replaced with best fitting constants. We thus attempt to mimic the work of Eberhart-Phillips et al., 1989, but derive all parameters as a simple function of porosity and clay content in an attempt to improve the time-lapse predictive capabilities. However, due to seismic velocity being a complex function of many rock properties, we find that the shape-curvature of the nonlinear relationships cannot be suitably described by porosity and clay content alone. As a result, substituting best fit constant with these simple relationship does not improve time-lapse velocity predictions for hydrocarbon scenarios across all models (e.g., Figure 9). A quick analysis of the equations of Eberhart-Phillips et al., 1989 show that improved time-lapse velocity predictions may be possible if you have knowledge of the time-lapse porosity change. We estimate that porosity changes on the order of $\approx 1\%$ need to be resolved to improve these predictions.

7 CONCLUSION

In this paper, we have analysed several non-linear stress-dependent rock physics models and examined their behaviour and stability when exposed to a large (dry) core dataset of different lithologies. We demonstrated, from a dataset of over 400 ultrasonic velocity versus stress core measurements, that all models can be calibrated using similar global search techniques to give a relatively good fit to the observed data. The final results provide a useful tool for setting a priori parameter constraints for future model inversions. We observe that some models fail to accurately fit both the P- and S-wave stress dependence simultaneously. This is due to their assumption of an increase in the V_P/V_S ratio (hence Poisson's ratio) with stress. A trait not seen for every sample in our dataset. Thus improvements to these models are necessary if quantitatively accurate predictions of anisotropy are to be made. Also highlighted in this study is the limitation of TOE models in their approximation of an exponential relationship as functions that lacks an exponential term. As a direct result they appear to overestimate time-lapse changes in velocity with stress compared to other models. We demonstrate that most model parameters are well constrained. However, the TOE inversions are ill-posed due to the simplification of the equations to an isotropic rock. These results are likely improved by including more multi-

directional data. We argue that all the models are difficult to parameterise without the availability of core data. Therefore, we derive simple relationships between each parameter, core porosity and clay content. However, we observe parameters that govern the shape/curvature of the nonlinear relationship to show little correlation to porosity and clay content. As a result parametrising models with simple porosity-clay relationships show limited capabilities in predicting time-lapse change in velocity. Future research into parameter relationships with other properties is suggested. Finally, TOE-2 model struggles to approximate the velocity-stress core data to the same accuracy as that of velocity depth data. This highlights a potential limitation in core data as a representation of the stress dependence of the subsurface. Although potentially difficult to investigate, its importance is of great significance if we wish to accurately interpret observed time-lapse anomalies.

ACKNOWLEDGMENTS

The authors would like to thank the Wolfson Multiphase Flow Laboratory of the University of Leeds for permission to use their extensive stress-velocity core dataset in this study. D. Price is supported by a scholarship funded by Total GRC and the School of Earth & Environment, University of Leeds. D. Angus acknowledges the Research Council UK (EP/K035878/; EP/K021869/1; NE/L000423/1) for financial support.

Lithology	Reference
Sandstone	Han et al, 1986. Jizba, 1991. He, 2006. King, 1966; King, 2002. Rojas, 2005. Hemsing, 2007. Grochau and Gurevich., 2008.
Tight sandstone	Al-Harasi et al., 2013.
Limestone	Nur and Simmons, 1969. Brown, 2002. Simmons and Brace, 1965.
Dolostone	Nur and Simmons, 1969. Brown, 2002.
Conglomerate	He, 2006.
Anhydrite	Hemsing, 2007.
Shale	Hemsing, 2007. Hornby, 1998. Johnston and Christensen, 1995. Lorinczi et al., 2014.
Granite	Nur and Simmons, 1969.
Carbonate	Hemsing, 2007.

Table 1. Published ultrasonic velocity-stress core data.

Model	Unkown model parameters
Empirical (EMP)	A_P, B_P, D_P, A_S, B_S, D_S
First Principle Model (FPR)	V_P^{gr}, V_S^{gr}, ϕ_c^0, a
Micro-structural Model (MST)	V_P^{gr}, V_S^{gr}, a^0, ϵ^0
Third Order Elasticity - 1 (TOE-1)	c_{111}, c_{112}, c_{123}
Third Order Elasticity - 2 (TOE-2)	A, B, C, V_{P0}, V_{S0}

Table 2. Unknown rock physics model paramters found via inversion of the ultrasonic velocity-stress core data.

$f(\phi, C) = X_0 + X_1\phi + X_2C$					
Model	Parameter	Coefficient			R^2
		X_0	X_1	X_2	
EMP	$A_{p/s}$	5594 / 3725	-7650 / -5842	-1143 / -1196	0.749 / 0.721
	$B_{p/s}$	1923 / 1114	-2393 / -410.2	-2070 / -1382	0.152 / 0.173
	$D_{p/s}$	5.370 / 3.581x10^{-8}	1.082 / 2.154 x10^{-7}	-3.853 / -9.537 x10^{-8}	0.056 /0.281
FPR	V_P^{gr}	5612	-7681	-1057	0.760
	V_S^{gr}	3670	-6038	-1085	0.716
	ϕ_c^0	6.212x10^{-4}	1.787x10^{-4}	9.426x10^{-6}	9. 193x10^{-4}
	a	2.560x10^{-4}	1.175x10^{-4}	1.478x10^{-4}	0.278
MST	V_P^{gr}	5570	-7594	-1044	0.751
	V_S^{gr}	3670	-6038	-1085	0.716
	a^0	1.731x10^{-4}	9.688x10^{-4}	1.258x10^{-3}	0.318
	ϵ^0	2.138x10^{-1}	-1.331x10^{-1}	-2.583x10^{-1}	0.069
TOE-2	V_{P0}	3499	-5131	1078	0.126
	$(A + 3B + C)$	-2.259x10^{13}	3.371x10^{13}	2.451x10^{13}	0.130

Table 3. Table showing the coefficients of the linear regression surface for each rock physics model parameter as a function of porosity ϕ and clay content C. The corresponding R^2 value for each surface is also included to indicate the goodness of fit. Note that all velocities, i.e. V_P^{gr} etc., are given in ms^{-1} and third order coefficients i.e. $(A + 3B + C)$, in Pascals.

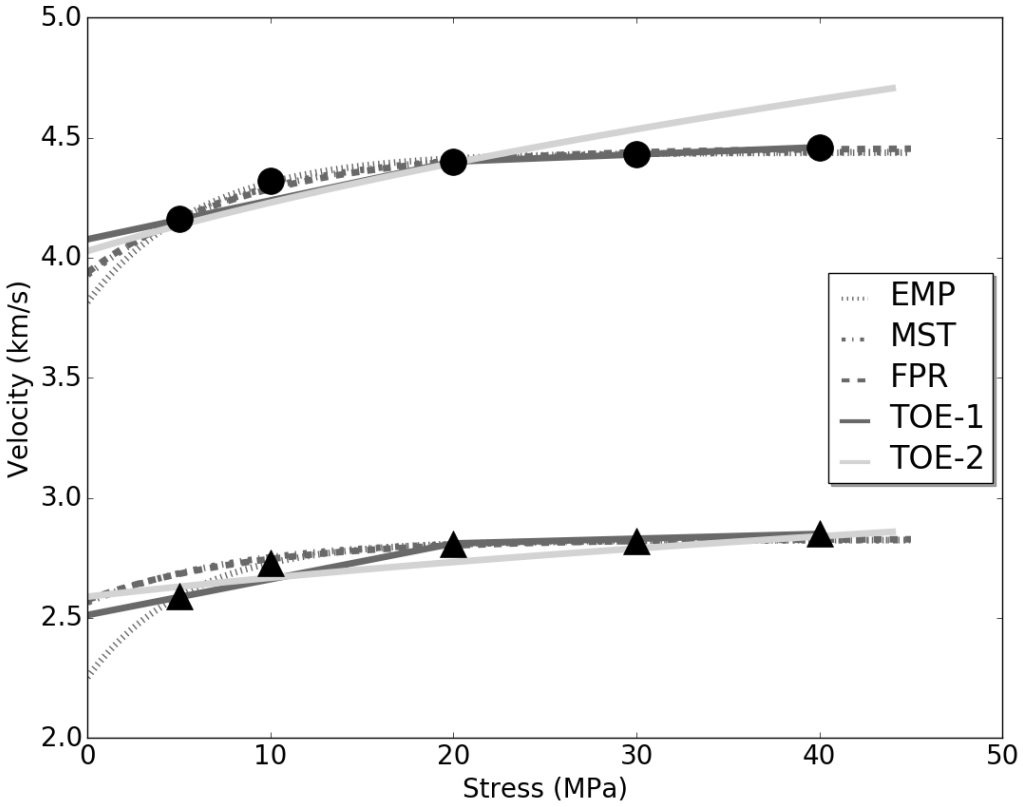

Figure 1. Rock physics model velocity-stress predictions for a representative sandstone core sample. Ultrasonic P-wave data shown by black circles and S-wave data by black triangles.

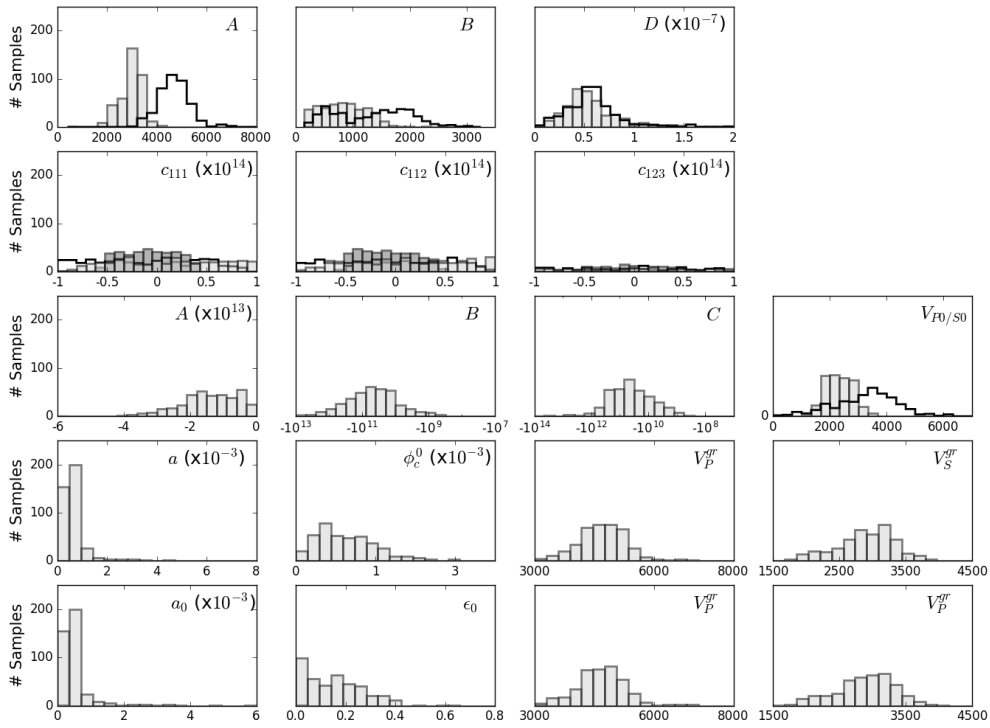

Figure 2. Histograms showing the range of inverted model parameters for all rock physics models: [top row] EMP model parameters, P-wave (line) and S-wave (bar); [second row] TOE-1 model, low stress regime (Line), middle stress regime (light grey bar) and high stress regime (dark grey bar); [third row] TOE-2, with V_{S0} displayed as a bar plot whilst V_{P0} a line; [fourth row] FPR model and [bottom row] MST model. Note that all velocities are given in ms^{-1} and third order coefficient in Pascals.

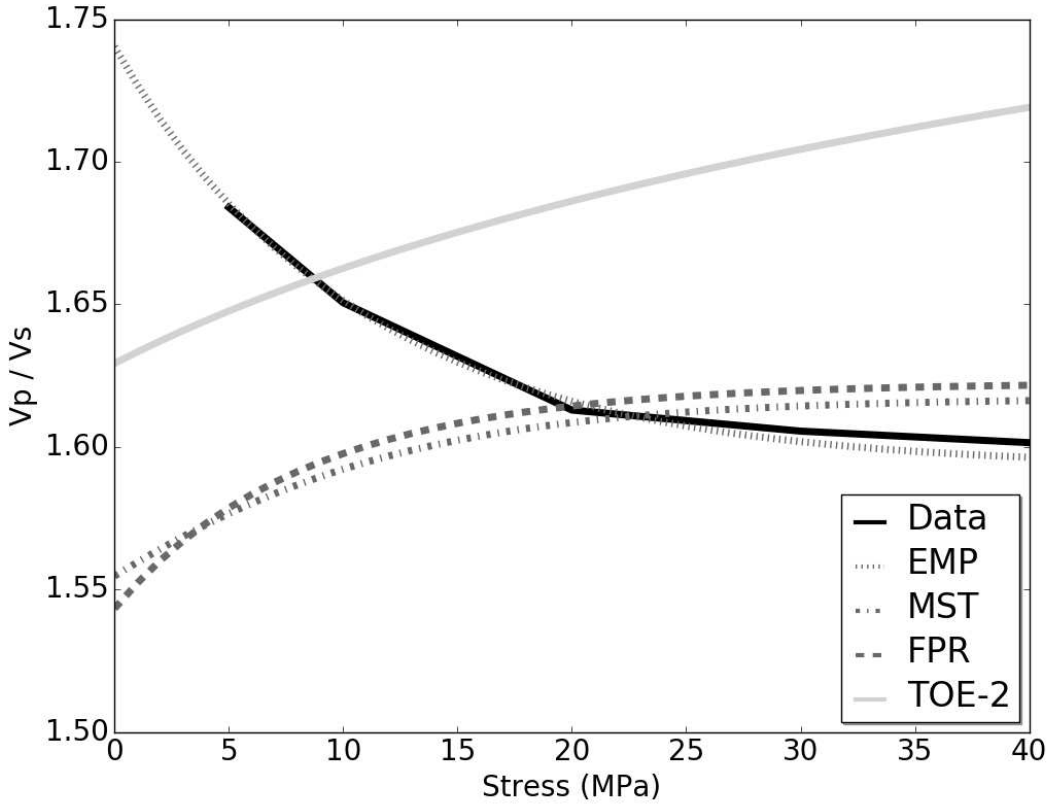

Figure 3. V_P/V_s ratio of the velocity-stress data for the representative sandstone sample of Figure 1 along with the corresponding ratios derived from the velocity-stress predictions of each rock physics model.

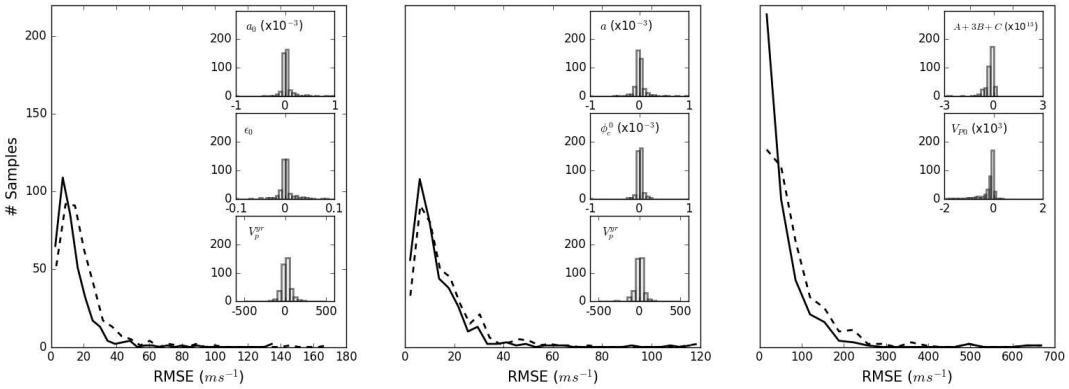

Figure 4. Histograms showing the range of Root-mean-square errors between the P-wave data and the rock physics model for all core samples. Dashed line represents those models derived from inverting both P- and S-waved data, whilst the solid line those derived from the P-wave data alone. Left is the MST, middle the FPR and right the TOE-2 model. The inset histograms show the absolute differences in the unknown parameters between each inversion. Note all velocities are given in ms^{-1} and the third order coefficients in Pascals.

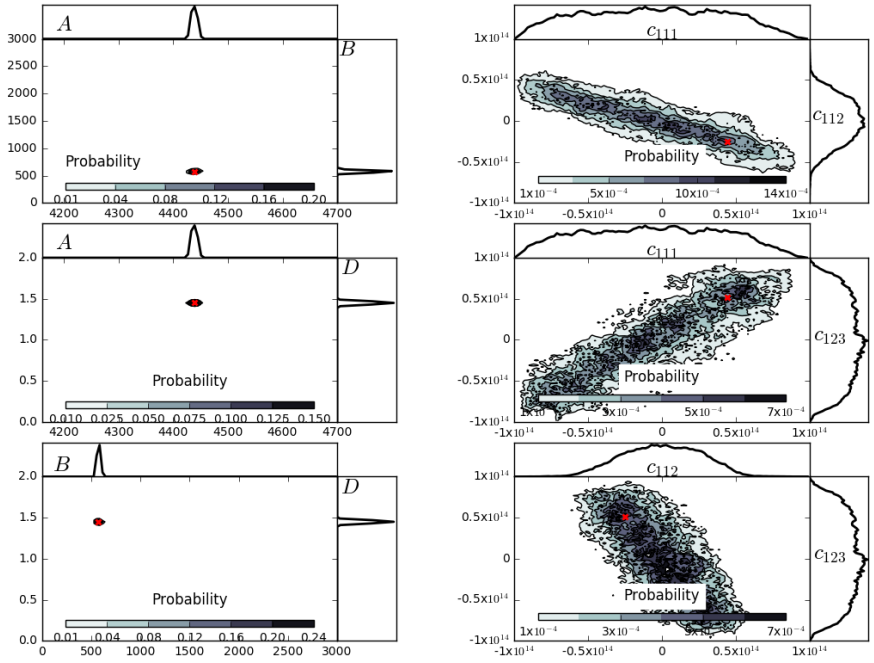

Figure 5. 1D and 2D Probability Density Functions (PDFs) for parameters A_ν, B_ν and D_ν of the P-wave EMP model (left) and parameters c_{111}, c_{112} and c_{123} of the TOE-1 model (right) for the representative sandstone sample of Figure 1. The red cross indicates the final inversion result used to plot the models displayed in Figure 1.

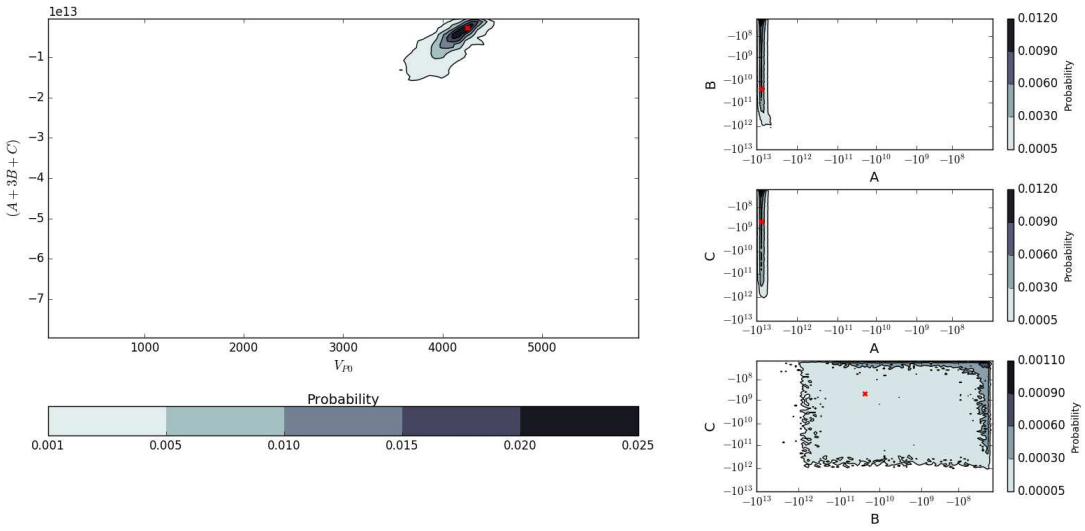

Figure 6. Left, the 2D PDF of the two unknown parameters, V_{P0} and $A + 3B + C$, of the P-wave only TOE-2 inversion. Right, the 2D PDF's when attempting to invert for each third order coefficient, A, B and C independently using both P- and S-wave data. Note that again these PDF's were created based on the results of the representative sandstone of Figure 1 with the red cross indicating the final inversion result.

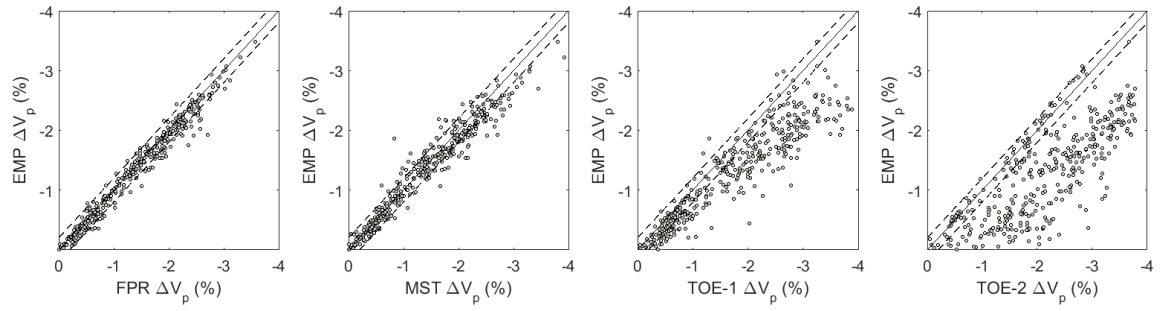

Figure 7. Crossplots of the percentage velocity change associated with 5MPa reduction in effective stress (i.e. 35 to 30MPa) predicted by each of the rock physics models for each core sample. A reduction in effective stress typically seen in hydrocarbon monitoring scenarios. The results of the EMP model are used as a reference due to it having the lowest RMSE for most core samples. Due to degradation of the FPR and MST model solutions when the S-wave data is considered, these results are based on the P-wave only inversion results. The dotted lines represent a +/- 0.2% velocity change region.

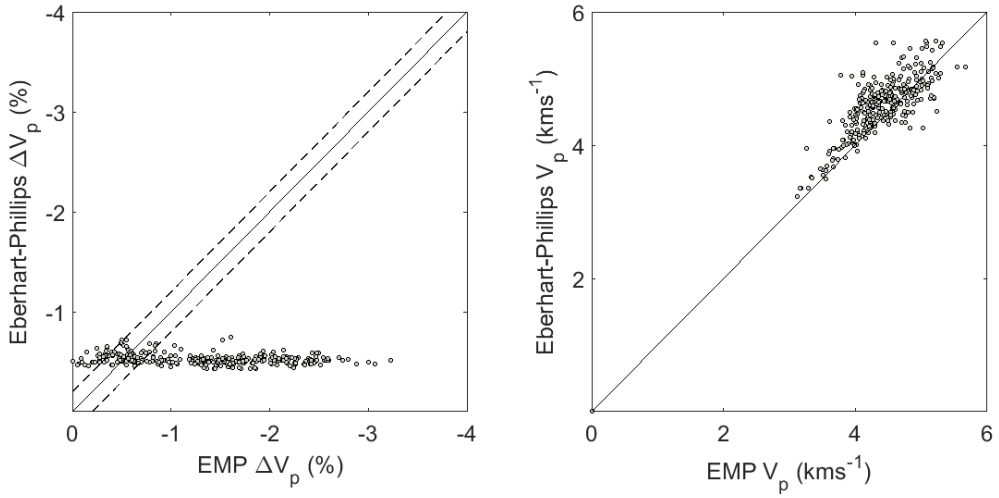

Figure 8. Crossplots showing the absolute P-wave velocity associated with 35MPa of effective stress for each sandstone core sample predicted by equation 32 against those of the EMP model (right). Also crossplotted is the percentage velocity change associated with a 5MPa reduction in effective stress (i.e. 35 to 30MPa) for each sandstone sample predicted by the two models (left). This represents the same hydrocarbon scenario as that of Figure 7. The dotted lines represent a +/- 0.2% velocity change region.

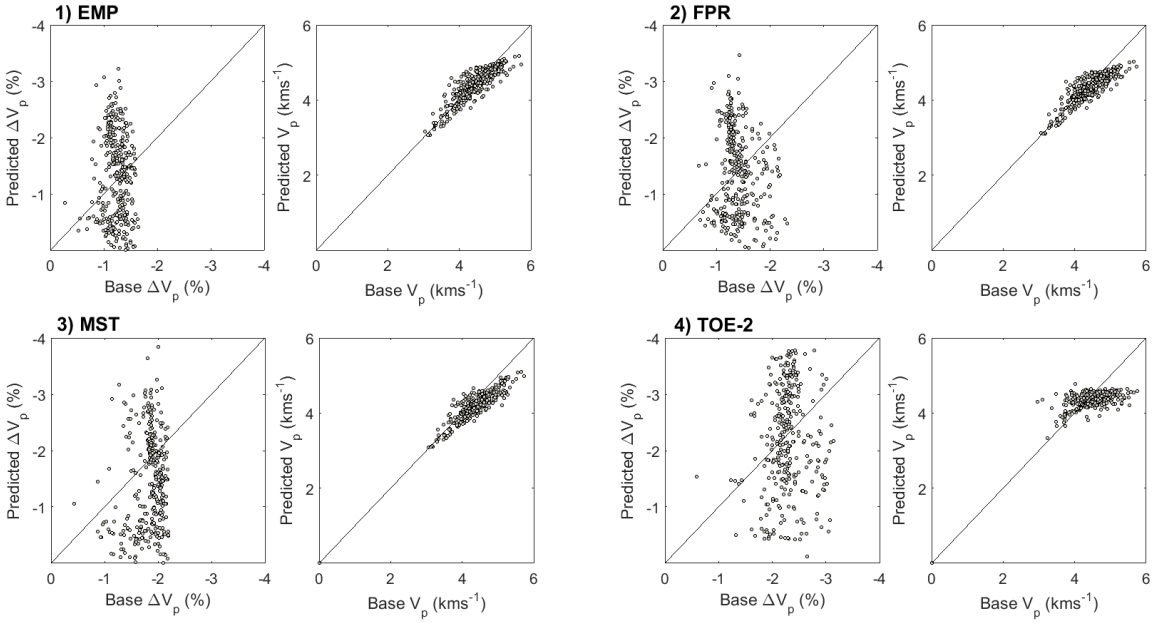

Figure 9. Crossplots showing the absolute velocity and percentage change associated with the hydrocarbon scenario of Figure 7, predicted by the linear regression surfaces of Table 3 against those predicted by the original inverted model (i.e. Base case).

REFERENCES

Al-Harrasi, M., Grattoni, C., Fisher, Q.J. and Lane, M. (2013) Gas condensate flow behaviour within tight reservoirs, *Society of Petroleum Engineers - SPE Middle East Unconventional Gas Conference and Exhibition*, 239-257.

Angus, D.A., Verdon, J.P., Fisher, Q.J. and Kendall, J.M. (2009) Exploring trends in microcrack properties of sedimentary rocks: An Audit of dry-core velocity-stress measurements, *Geophysics*, **74**(5), E193-E203.

Angus, D.A., Fisher, Q.J. and Verdon, J.P. (2012) Exploring trends in microcrack properties of sedimentary rocks: An audit of dry and water saturated sandstone core velocity-stress measurements, *International Journal of Geosciences*, **3**, 822-833.

Angus, D.A., Dutko, M., Kristiansen, T.G., Fisher, Q.J., Kendall, J.M., Baird, A.F., Verdon, J.P., Barkved, O.I., Yu, J. and Zhao, S. (2015) Integrated hydro-mechanical and seismic modelling of the Valhall reservoir: A case study of predicting subsidence, AVOA and microseismicity, *Geomechanics for Energy and the Environment*, **2**, 32-44.

Arts, R.J., Rasolofosaon, N.J.P. and Zinszner, B.E. (1992) Experimental determination of the complete anisotropic viscoelastic tensor in rocks, *SEG Expanded Abstracts*, RP 1.7.

Avseth, P., Mukerji, T. and Mavko, G. (2010) Quantitative Seismic Interpretation: Applying Rock Physics Tools to Reduce Interpretation Risk, *Cambridge University Press*, Cambridge, pp. 7359.

Baird, A.F., Kendall, J.M. and Angus, D.A. (2013a) Frequency dependent seismic anisotropy due to fracture: fluid flow versus scattering, *Geophysics*, **78**(2), WA111-WA122.

Baird, A.F., Kendal, J.M., Verdon, J.P., Wuestefeld, A., Noble, T.E., Li, Y., Dutko, M. and Fisher, Q.J. (2013b) Monitoring increases in fracture connectivity during hydraulic stimulations from temporal variations in shear-wave splitting polarization, *Geophysical Journal International*, **195**(2), 1120-1131.

Brown, L. (2002) Integration of rock physics and reservoir simulation for the interpretation of time-lapse seismic data at Weyburn field, Saskatchewan, *M.Sc. dissertation*, Colorado School of Mines.

Choi, M.K., Pyrak-Nolte, L.J., and Bobet, A. (2014) The effect of surface roughness and mixed-mode loading on the stiffness ratio K_x/K_z for fractures, *Geophysics*, **79**(5), D319-D331.

Cornet, F.H. (2015) Elements of Crustal Geomechanics, *Cambridge University Press*, Cambridge, p.461.

Crampin, S. (2005) A review of shear-wave splitting in the compliant crack critical anisotropic Earth, *Wave Motion*, **41**(1), 59-77.

De Genarro, S., Schutlensm P., Frumau, M. and Fuery, M. (2010) The role of geomechanics in the development of an HPHT field, *American Rock Mechanics*, 44th US Rock Mechanics Symposium.

Donald, J.A. and Prioul, R. (2015) In situ calibrated velocity-to-stress transforms using shear sonic radial profiles for time-lapse production analysis, *The Leading Edge*, 936-942.

Dvorkin, J., Gutierrez, M.A. and Grana, D. (2014) Seismic Reflections of Rock Properties, *Cambridge University Press*, Cambridge, pp.324.

Eberhart-Phillips, D., Han, D-H. and Zoback M. D. (1989) Epiricle relationships among seismic velocity, effective pressure, porosity, and clay content in sandstone, *Geophysics*, **54**(1), 82-89.

Fuck, R.F., Tsvankin, I. (2009) Analysis of the symmetry of a stressed medium using nonlinear elasticity, *Geophysics*, **74**(5), 79-87.

Grochau, M., and Gurevich, B. (2008) Investigation of core data reliability to support time-lapse interpretation in Campos basin, Brazil, *Geophysics*, **73**(2), E59-E65.

Guéguen, Y. and Sarout, J. (2011) Cahracteristics of anisotropy and dispersion in cracked medium, *Tectonophysics*, **503**, 165-172.

Guilbot, J. and Smith, B. (2002) 4-D constrained depth conversion for reservoir compaction estimation: Application to Ekofisk field, *The Leading Edge*, **21**, 302-308.

Hall, S., Kendall, J.M., Maddock, L. and Fisher, Q.J. (2008) Crack density tensor inversion for analysis of changes in rock frame architecture, *Geophysical Journal International*, **173**, 577–592.

Han D.H., Nur, A. and Morgan, D. (1986) Effects of porosity and clay content on wave velocities in sandstones, *Geophysics*, **51**(11), 2093-2107.

Hatchell, P. and Bourne, S. (2005) Rocks under strain: Strain-induced time-lapse time shifts are observed for depleting reservoirs, *The Leading Edge*, **24**, 1222.

He, T. (2006) P- and S-wave velocity measurement and pressure sensitivity analysis of AVA response, *M.Sc. dissertation*, University of Alberta.

He, Y., Angus, D.A., Blanchard, T., Garcia, A. (2016) Time-lapse seismic waveform modeling and seismic attribute analysis using hydro-mechanical models for a deep reservoir undergoing depletion, *Geophysical Journal International*, **205**, 389-407.

Hemsing, D. (2007) Laboratory determination of seismic anisotropy in sedimentary rock from western sedimentary rock from the western sedimentary basin, *M.Sc. dissertation*, University of Alberta.

Herwanger, J. and Koutsabeloulis, N. (2011) Seismic Geomechanics: How to Build and Calibrate Geomechanical Models Using 3D and 4D Seismic Data, *EAGE*.

Hornby, B.E. (1998) Experimental laboratory determination of the dynamic elastic properties of drained shales, *Journal of Geophysical Research: Solid Earth*, **103**(B12), 29945-29964.

Jizba, D. (1991) Mechanical and acoustic properties of sandstones and shales, *Ph.D. dissertation*, Stanford University.

Johnstion, D.H. (2013) Practical Applications of Time-lapse Seismic Data, *Society of Exploration Geophysicists*, pp. 270.

Johnston, J., and Christensen, N. (1995) Seismic anisotropy of shales, *Journal of Geophysical Research*, **100**(B4), 5991-6003.

Jones, S.M. (1995) Velocities and quality factors of sedimentary rocks at low and high effective pressures, *Geophysical Journal International*, **123**, 774-780.

Kendall, J.M., Fisher, Q.J., Crump, S., Maddock, J., Carter, A., Hall, S., Wookey, J., Valcke, S., Casey, M., Lloyd, G. and Ismail, W. (2007) Seismic anisotropy as an indicator of reservoir quality in siliclastic rocks, *Geological Society of London*, Special Publication, **292**, 123-136.

Khaksar, A., Griffiths, C.M., and McCann, C. (1999) Compressional and shear-wave velocities as a function

of confining stress in dry sandstone, *Geophysical Prospecting*, **47**, 487-508.

King, M. (1966) Wave velocities in rocks as a function of changes in overburden pressure and pore fluid saturants, *Geophysics*, **31** 50-73.

King, M. (2002) Elastic wave propagation and permeability for rocks with multiple parallel fractures, *International Journal of Rock Mechanics and Mining Sciences*, **39**, 1033-1043.

Kirkstetter, O and MacBeth, C. (2001) Compliance-based interpretation of dry fram pressure sensitivity in shallow marine sandstone, *Expanded Abstracts: Society of Exploration Geophysics, 71st Annual meeting*, 2132-2135.

Korneev, V and Glubokovskikh, S. (2013) Seismic velocity changes caused by an overburden stress, *Geophysics*, **78**(5), 25-31.

Lei, T., Sinha, B.K., and Sanders, M. (2012) Estimation of horizontal stress magnitudes and stress coefficients of velocities using borehole sonic data, *Geophysics*, **77**(3), WA181-WA196.

Lorinczi, P., Burns, A.D., Lesnic, D., Fisher, Q.J., Crook, A.J., Grattoni, C. and Rybalcenko, K. (2014) Direct and inverse methods for determining gas flow properties of shale, *Society of Petroleum Engineers*, 1-26.

Makse H.A., Gland, N., Johnson, D.L. and Schwartz, L.M. (1999) Why effective medium theory fails in granular materials, *Physical Review Letters*, **83**, 5070-5073.

Nasseri, M.H.B., Goodfellow, S.D., Wanne, T. and Young, R.P. (2013) Thermo-hydro-mechanical properties of Cobourg limestone, *International Journal of Rock Mechanics and Mining Sciences*, **61**, 212-222.

Nur, A. and Simmons, G. (1969) Stress-induced velocity anisotropy in rock: an experimental study, *Journal of Geophysical Research*, **74**, 6667-6674.

Ougier-Simonin, A., Sarout, J. and Guéguen, Y. (2009) A simplified model of effective elasticity for anisotropic shales, *Geophysics*, **74**, 57-63.

Prioul, R., Bakulin, A. and Bakulin, V. (2004) Nonlinear rock physics model for estimation of 3D subsurface stress in anisotropic formations, *Geophysics*, **69**, 415-425.

Rojas, M. (2005) Elastic rock properties of tight gas sandstones for reservoir characterization at Rulison fieild, Colorado, *M.Sc. dissertation*, Colorado School of Mines.

Roste, T., Stovas, A. and Landro, M. (2006) Estimation of layer thickness and velocity changes using 4D prestack seismic data, *Geophysics*, **71**, S219-S234.

Sambridge, M. (1999a) Geophysical inversion with a neighborhood algorithm: I, searching a parameter space, *Geophysical Journal International*, **138**, 479-494.

Sambridge, M. (1999b) Geophysical inversion with a neighborhood algorithm: II, appraising the ensemble, *Geophysical Journal International*, **138**, 727-746.

Sarout, J., Delle Piane, C., Nadri, D., Esteban, L. and Dewhurst, D.N.(2015) A robust experimental determination of Thomsen's δ parameter, *Geophysics*, **80**, 19-24.

Sarout, J., Esteban, L., Delle Piane, C., Maney, B. and Dewhurst, D.N.(2015) Elastic anisotropy of Opalinus Clay under variable saturation and triaxial stress, *Geophysical Journal International*, **198**, 1662-1682.

Sarout, J. and Guéguen, Y. (2008) Anisotropy of elastic wave velocities in deformed shales: Part 2-Modelling

results, *Geophysics*, **73**, 91-103.

Sayers, C.M. (2002) Stress-dependent elastic anisotropy of sandstones, *Geophysical Prospecting*, **50**, 85-95.

Sayers, C.M. and Kachanov, M. (1995) Microcrack induced elastic wave anisotropy of brittle rocks, *Journal of Geophysical Research*, **100**, 4149-4156.

Schoenberg, M. and Sayers, C.M. (1995) Seismic anisotropy of fractured rock, *Geophysics*, **60**, 204-211.

Schön, J.H. (1996) Physical Properties of Rocks: Fundamentals and Principles of Petrophysics, *Handbook of Geophysical Exploration: Seismic Exploration*, Elsevier, London, pp. 583.

Schubnel, A., and Gueguen, Y. (2003) Dispersion and anisotropy of elastic waves in cracked rocks, *Journal of Geophysical Research*, **108**(B2), ESE16.1-ESE16.15.

Shapiro, S. (2003) Elastic piezosensitivity of porous and fractured rocks, *Geophysics*, **68**, 482-486.

Shapiro, S. and Kaselow, A. (2005) Porosity and elastic anisotropy of rocks under tectonic stress and pore-pressure changes, *Geophysics*, **70**, no.5, N27-N38.

Simmons, G. and Brace, W. (1965) Comparison of static and dynamic measurements of compressibility of rocks, *Journal of Geophysical Research*, **70**, 5649-5656.

Sinha, B.K. and Plona, T.J. (2001) Wave propagation in rocks with elastic-plastic deformations, *Geophysics*, **66**(3), 772-785.

Terzaghi, K. (1943) Theoretical Soil Mechanics, *John Wiley and Sons*, New York.

Thurston, R.N. and Brugger, K. (1964) Third-order elastic constants and the velocity of small amplitude elastic waves in homogeneously stressed media, *Physical Review*, **133**(6A), A1604-A1610.

Tod, S.R. (2002) The effects of stress and fluid pressure on the anisotropy of interconnected cracks, *Geophysical Journal International*, **70**, no.5, N27-N38.

Verdon, J., Angus, D.A., Kendall, J.M. and Hall, S. (2008) The effects of microstructure and nonlinear stress on anisotropic seismic velocities, *Geophysics*, **73**(4), D41–D51.

Verdon, J.P. and Wüstefeld, A. (2013) Measurement of the normal/tangential fracture compliance ratio (Z_N/Z_T) during hydraulic fracture stimulation using S-wave splitting data, *Geophysical Prospecting*, **61**, 461-475.

Walsh, J. (1965) The effect of cracks on the compressibility of rock, *Journal of Geophysical Research*, **70**, 381–389.

Walsh, J. (1965b) The effect of cracks on the uniaxial elastic compression of rocks, *Journal of Geophysical Research*, **70**, 399-411.

Yousef, B. and Angus, D.A. (2016) When do fractured media become seismically anisotropic? Some implications on quantifying fracture properties, *Earth and Planetary Science Letters*, **444**, 150-159.

Zimmerman, R.W., Somerton, W.H. and King, M.S. (1986) Compressibility of porous rocks, *Journal of Geophysical Research*, **91**, 12765-12777.

Zoback, M. D. (2010) Reservoir Geomechanics,, *Cambridge University Press*, Cambridge, p. 449.